Recombinant human bone morphogenetic protein-7 enhances bone formation ability of jaw bone defect using human umbilical cord mesenchymal stem cells combined with nano-hydroxyapatite/collagen/poly(L-lactide)

E Lingling
Chinese PLA General Hospital https://orcid.org/0000-0003-1955-9851
Helin Xin
Chinese PLA General Hospital
Xing Wang
Chinese PLA General Hospital
Tao Cheng
Chinese PLA General Hospital
Shou Zhang
Chinese PLA General Hospital
Xiaocao Ma
Chinese PLA General Hospital
Rong Zhang
Chinese PLA General Hospital
Hongchen Liu (liu-hc301@hotmail.com)
Chinese PLA General Hospital

Research

Keywords: recombinant human bone morphogenetic protein-7, human umbilical cord mesenchymal stem cells, nano-hydroxyapatite/collagen/poly(L-lactide), bone tissue engineering, jaw bone defect

Posted Date: October 2nd, 2020

DOI: https://doi.org/10.21203/rs.3.rs-85305/v1

Abstract

Background: Human umbilical cord mesenchymal stem cells (hUC-MSCs) have been suggested as an alternative source of MSCs. However, the studies on its bone formation ability in oral maxillo-facial bone defect are rare. This study investigated the bone formation ability of recombinant human bone morphogenetic protein-7 (rhBMP-7)-induced hUC-MSCs combined with nano-hydroxyapatite/collagen/poly(L-lactide) (nHAC/PLA) in the back of nude mice and jaw bone defect of rabbit.

Methods: The characteristics of hUC-MSCs were analyzed by plastic adherence, cell phenotype and multilineage differentiation potential. Cell proliferation was examined using a CCK-8 assay. Osteogenic differentiation was evaluated by quantitative calcium concentration, phosphorous concentration, alkaline phosphatase (ALP) activity, osteocalcin (OCN) concentration, mineral formation, and the mRNA levels of ALP, OCN and bone morphogenetic protein (BMP)-2. Scanning electron microscopy was used to observe cell adhesion, growth and differentiation. Bone formation was assessed by immunohistochemical staining, micro-CT and hematoxylin and eosin staining.

Results: The isolated hUC-MSCs expressed CD105, CD90 and CD73, did not express CD45, CD34, CD11a and HLA-DR, exhibited self-renewal potential, and favored osteogenesis and adipogenesis. The exogenously-added rhBMP-7 attenuated the inhibitory effect of the serum-free osteogenic media (OMD) on the proliferation of hUC-MSCs combined with nHAC/PLA, increased the promoting effect of OMD on osteogenic differentiation of hUC-MSCs in two or three-dimensional culture, and enhanced its heterotopic bone formation and jaw bone defect repair abilities. Furthermore, the bone formation of *in situ* bone defect was significantly superior to heterotopic bone formation.

Conclusions: That the microenvironment formed by the regenerative engineered constructs and the *in situ* bone defect microenvironment closely matched that of the bone tissue in its native state may be essential for sufficient and timely bone regeneration. The endogenously-produced BMPs may serve an important regulatory role in the process. These results paved the way for developing allogeneic hUC-MSCs-based constructs for clinical jaw bone regenerative therapeutic applications.

Introduction

Oral maxillo-facial bone defects affect human chewing, pronunciation, digestion, appearance and movement, thus affecting the mental and general health of patients [1]. Autologous bone grafts are frequently used to treat these bone defects caused by surgical resection, congenital defects, chronic infection or trauma in the clinic. However, autologous bone grafts have critical limitations, such as insufficient bone mass, donor site morbidity and requirement of a second surgery [2]. The stem cell-based tissue-engineering technique is a promising approach to avoid these problems using scaffold alone or in combination with growth factor and/or stem cells [3]. Therefore, it is important to select the appropriate scaffold, stem cell and growth factor to build tissue-engineered constructs suitable for clinical application

in bone tissue engineering. Human bone marrow-derived mesenchymal stem cells (hBM-MSCs) possessing broad characteristics of MSCs are currently regarded as the “gold standard” among MSCs [4]. However, the harvest of hBM-MSCs requires an invasive procedure, and hBM-MSCs have a lower self-renewal potential with aging [5–7].

A study has shown that MSCs may exist in all vascularized tissue in the entire body [8]. Human umbilical cord mesenchymal stem cells (hUC-MSCs) from Wharton’s jelly have been suggested as an alternative source of MSCs, due their unique combination of prenatal and postnatal stem cell properties [9]. hUC-MSCs have a higher expression of pluripotent markers compared with hBM-MSCs [10–12], but a lower expression compared with human embryonic stem cells (hESCs) [13, 14]. Different from hESCs [15] and hBM-MSCs [16], hUC-MSCs, being non-tumorigenic, have a high potential for safe cell-based therapies. They have a low cost, inexhaustible cell sources, high plasticity and developmental flexibility, and do not produce immune rejection during transplantation [17]. Numerous studies have demonstrated that hUC-MSCs can differentiate into osteoblasts, adipocytes, chondrocytes, endothelial cells and neurons under specific culture conditions [18–24]. To date, the Food and Drug Administration (FDA) has registered some clinical trials (phases 1–3) to assess the safety and efficacy of unmodified hUC-MSCs for the treatment of osteoarthritis [9]. Compared with hBM-MSCs or human adipose tissue-derived mesenchymal stem cells, hUC-MSCs can form more calcium nodules when induced by osteogenic factor for 35 days [25]. In addition, the proliferative potential of hUC-MSCs is higher compared with that of hBM-MSCs or MSCs from other postnatal and neonatal sources [25–29].

During normal fracture healing, bone morphogenetic proteins (BMPs) and regulatory cytokines can promote the proliferation of undifferentiated MSCs and thus induce them to differentiate into chondrocytes and osteoblasts to form bone and repair damage [30–32]. BMP-7 has been reported to promote bone healing in spinal fusion, fracture repair and distraction osteogenesis in animals and humans [32, 33], and it has been approved by the FDA for adjuvant treatment of various clinical musculoskeletal diseases [34]. Early experiments also demonstrated that recombinant human BMP-7 (rhBMP-7) can individually induce all types of mesenchymal precursor cells into chondroblasts or osteoblasts [35, 36]. Edgar [36] reported that exogenously-added BMP-7 enhances osteogenic differentiation of BM-MSCs by promoting the expression of endogenous BMP profiles. However, to the best of our knowledge, the effect of exogenously-added rhBMP-7 on the osteogenic differentiation of hUC-MSCs is not yet fully understood.

Nano-hydroxyapatite/collagen/poly(L-lactide) (nHAC/PLA), a developed ceramic/polymer composite material, mimics the nano-to microscale hierarchical microstructure of natural, cancellous bones [37]. It is composed of hydroxyapatite, a type of collagen and polylactic acid, with a porosity of 70–88% and a pore size range of 300 ± 250 nm. The content of hydroxyapatite is 45 ± 5%, and the mechanical properties and strength are similar to natural, cancellous bones. nHAC/PLA is often used for alveolar ridge extension and jaw bone defect filling [38]. Our previous and other studies have supported the use of nHAC/PLA in periodontal and other types of bone regeneration [38–40].

Hence, the combination of hUC-MSCs, rhBMP-7 and nHAC/PLA was used in the present study to construct tissue engineered bones for the repair of jaw bone defect in New Zealand rabbits *in vivo*. The aim of the present study was to engineer a three- dimensional allogeneic hUC-MSCs-based construct to study its potential for clinical jaw bone regenerative therapeutic applications.

Materials And Methods

Harvest and culture of hUC-MSCs

An explant culture method [41] was used to culture hUC-MSCs. All surgical procedures and care administered to human samples were approved by the Medical Ethics Committee of Chinese People's Liberation Army (PLA) General Hospital (ethics approval no. S2018-093-01). Briefly, after informed consent in writing was obtained, 10 umbilical cord tissues from 10 healthy individuals with full-term pregnancy (age, 25–32 years) were collected and minced into small sections. All samples were obtained from the Maternity Department of Chinese PLA General Hospital (Beijing, China). Following the removal of the vascular, perivascular and epithelial tissues of every small section, the remaining Wharton's Jelly was minced into 1 cm^3 fragments. The fragments were then attached to the bottom of a culture dish and incubated at 37˚C in 5% CO_2, from which the hUC-MSCs migrated in the human MSC serum-free medium containing 500 ml human MSC serum-free basal medium (catalog no. CM-SC01; Procell Life Science technology Co., Ltd.), 25 ml human MSC serum-free medium growth additives (catalog no. CM-SC01; Procell Life Science technology Co., Ltd.) and 5 ml gentamicin-streptomycin solution (catalog no. CM-SC01; Procell Life Science technology Co., Ltd.). The third passage cells were used to perform a series of experiments.

Proliferative potential of hUC-MSCs

The hUC-MSCs were plated into 96-well culture plates at a density of 2×10^4 cells/ml, and then were cultured in 100 µl human MSC serum-free medium for 1–10 days to test their proliferative potential using a Cell Counting Kit-8 (CCK-8), according to the manufacturer's protocol (catalog no. 35002; Dojindo Molecular Technologies, Inc.).

Phenotype of hUC-MSCs

Flow cytometry was used to analyze the phenotype of hUC-MSCs. Trypsinized cells were suspended in phosphate-buffered saline (catalog no. PBS-10001; Cyagen Biosciences, Inc.) at a density of 5×10^6 cells/ml, and a 100 µl sample was incubated with various BD Pharmingen™ PE Mouse anti-Human CD73 (catalog no. 561014; 1:50), CD105 (catalog no. 560839; 1:50), CD34 (catalog no. 560941; 1:50) and BD Pharmingen™ FITC Mouse anti-Human CD90 (catalog no. 561969; 1:50), CD45 (catalog no. 560976; 1:50), CD11a (catalog no. 555383; 1:50) and HLA-DR catalog no. 560944; 1:50) antibodies (BD Biosciences) for 45 min at room temperature. Control samples were incubated with PBS instead of antibodies. Antibody binding was examined using a FACScan flow cytometer (Beckman Coulter) and was analyzed using FlowJo v10.6.2 (BD Biosciences).

Osteogenic differentiation potential of hUC-MSCs

Osteogenic differentiation was induced in hUC-MSCs by Oricell™ hUC-MSCs osteogenic differentiation medium kit (catalog no. HUXUC-90021; Cyagen Biosciences, Inc.). The cells were seeded in 24-well culture plates at a density of 1×10^4 cells/cm^2 and cultured in the human MSC serum-free medium. When confluence recached 80–90%, the cells were cultured in hUC-MSCs osteogenic differentiation medium for 21 days, and then were fixed with 4% neutral formaldehyde for 30 min at room temperature. The extracellular matrix calcification was examined using Alizarin red staining for 5 min at room temperature. The stained cells were photographed under an inverted light microscope.

Adipogenic differentiation potential of hUC-MSCs

Adipogenic differentiation was induced in hUC-MSCs by Oricell™ hUC-MSCs adipogenic differentiation medium kit (catalog no. HUXUC-90031; Cyagen Biosciences Inc, USA). The cells were plated onto chamber slides in 6-well plates at a density of 2×10^4 cells/cm^2 and cultured in the human MSC serum-free medium. When confluence reached 100%, the cells were cultured in hUC-MSCs adipogenic differentiation medium for 21 days, and then were fixed with 4% neutral formaldehyde for 30 min at room temperature and examined with Oil red O staining for 30 min at room temperature. The stained cells were photographed under an inverted light microscope.

Effect of rhBMP-7 on the osteogenic differentiation of hUC-MSCs seeded on culture plates

The hUC-MSCs were seeded onto chamber slides in 24-well culture plates or 24-well culture plates at a density of 1×10^5 cells/cm^2 and were cultured in the human MSC serum-free medium. When confluence reached 80–90%, the cells were cultured in 1 ml human MSC serum-free medium, 1 ml human MSC serum-free OMD, or 1 ml human MSC serum-free OMD supplemented with 100 ng/ml rhBMP-7 (catalog no. 354-BP-010/CF; R&D Systems, Inc.) [36]. The serum-free Oricell™ hUC-MSCs osteogenic differentiation medium served as OMD. On day 14 of differentiation, the cells were fixed with 4% neutral formaldehyde for 30 min at room temperature. Immunofluorescence staining was used to examine the expression of OCN. Simply, the cells were incubated with mouse anti-human OCN monoclonal antibody (catalog no. MAB1419; 1:50; R&D Systems, Inc.) overnight at 4˚C. FITC-conjugated anti-rabbit IgG secondary antibody (1:50; Santa Cruz Biotechnology, Inc.) was applied for 2 h at room temperature. The nucleus was stained with 4',6-diamidino-2-phenylindole (Merck KGaA) for 15 min at room temperature. Subsequently, the confocal images were recorded using a confocal microscope.

The Gomori calcium-cobalt method [40] was then used to estimate alkaline phosphatase (ALP) activity. The mineral formation was examined using Alizarin red staining for 5 min at room temperature. The stained cells were photographed under an inverted light microscope. For mineral formation measurements, each well was eluted for 30 min at room temperature with 1 ml 10% acetic acid solution on the rocking bed. The absorbance values of the eluent were then measured at 490 nm using a microplate reader [40].

Preparation and seeding of nHAC/PLA scaffolds

The nHAC/PLA materials (Beijing Allgens Medical Science & Technology Co., Ltd.) were constructed into blocks of 3.5 × 3.5 × 3.5, 5 × 5 × 5 and 10 × 4 × 3 mm. The samples were rinsed with 100% alcohol and sterilized with cobalt 60. The hUC-MSCs were seeded onto nHAC/PLA in 24-well plates and cultured in the human MSC serum-free medium for 24 h at 37˚C, allowing the cells to adhere to nHAC/PLA. The medium was then changed to additional human MSC serum-free medium, human MSC serum-free OMD or human MSC serum-free OMD supplemented with 100 ng/ml rhBMP-7. The constructs were then ready for a series of experiments.

Scanning electron microscopy

The hUC-MSCs were seeded onto 10 × 4 × 3 mm nHAC/PLA scaffolds in 24-well plates at a density of 1×10^7 cells/cm^2 per sample and were cultured in 1 ml mentioned above medium for 7 days. The constructs were fixed with 2% paraformaldehyde and 2.5% glutaraldehyde (Merck KGaA) in 0.1 mol/l phosphate buffer for 48 h at room temperature, and were then rinsed with PBS, different concentrations of ethanol, and different concentrations of hexamethyldisilazane. The construct were glued with conducing paste (catalog no. C680548; 8 mmx20 m; Nissin EM Co., Ltd.) to appropriate mounting stabs and coated with a several nanometer-thick layer of gold and examined under a Hitachi S-520 scanning electron microscope.

Effect of rhBMP-7 on the proliferation of hUC-MSCs combined with nHAC/PLA

The hUC-MSCs were seeded onto 3.5 × 3.5 × 3.5 mm nHAC/PLA scaffolds in 96-well plates at a density of 2×10^4 cells/cm^2 per sample and were cultured in 100 µl mentioned above medium for 1, 3, 5, 7 and 9 days to measure the proliferation of hUC-MSCs using CCK-8 according to the manufacturer's protocol (catalog no. 35002; Dojindo Molecular Technologies, Inc.).

Effect of rhBMP-7 on the osteogenic differentiation of hUC-MSCs combined with nHAC/PLA

The hUC-MSCs were seeded onto 5 × 5 × 5 mm nHAC/PLA scaffolds in 24-well plates at a density of 1×10^6 cells/cm^2 per sample and were cultured in 1.5 ml mentioned above medium for 7 and 14 days. The medium was then collected from the wells to measure calcium (Ca) concentration [catalog no. 05168449190; Calcium Gen.2 (Ca 2) kit; Roche Diagnostics GmbH] phosphorous (P) concentration [catalog no. 05171377190; Phosphate (Inorganic) ver.2 (PHOS2) kit; Roche Diagnostics GmbH], ALP activity (catalog no. 03333701190; Alkaline Phosphatase acc. to IFCC Gen.2 kit; Roche Diagnostics GmbH) and OCN concentration (catalog no. 12149133122; Elecsys N-MID Osteocalcin kit; Roche Diagnostics GmbH) using an automatic biochemical analyzer (Roche COBAS8000; Roche Diagnostics GmbH) in the Biochemistry Department of Chinese PLA General Hospital. On day 14 of culture, the constructs were examined using Alizarin red staining for 5 min at room temperature and photographed. For mineral formation measurements, each construct was eluted for 30 min at room temperature with 1 ml 10% acetic acid solution on the rocking bed. The constructs were then removed and the absorbance value of the eluent was measured at 490 nm using a microplate reader. The nHAC/PLA without cells was used as a blank control. The absorbance value of the blank control well was subtracted from the experimental well points to control stain retention.

Total cellular RNA was then extracted from the constructs with TRIzol reagent (catalog no. 15596-018; Thermo Fisher Scientific, Inc.), and reverse-transcribed into cDNA using a Reverse Transcription kit (catalog no. A5001; Promega Corporation) with annealing at 25˚C for 5 min, extension at 42˚C for 60 min and inactivating at 70˚C for 15 min. SYBR® Green Real-time polymerase chain reaction Master mix (catalog no. QPK-201; Toyobo Life Science) was used to quantify the target genes, including ALP, OCN, BMP-2 and GAPDH. Simply, the components of the PCR system were added and uniformly mixed to 20 μl, with 95˚C of pre-denaturation for 5 min, followed by qPCR, with denaturation at 95˚C for 10 sec, annealing at 60˚C for 30 sec, and extension at 72˚C for 30 sec. A total of 40 cycles were performed. The $2^{-\Delta\Delta Cq}$ method [42] was used to evaluate relative gene expression normalized by the C_q of the housekeeping gene GAPDH. The C_q value of hU-CMSCs + nHAC/PLA cultured in serum-free medium for 7 days served as the calibrator (biological replicates, n = 3; technical replicates, n = 3). The primer sequences are listed in Table 1.

Table 1
Sequences of primers used for RT-PCR and the product size

Gene	Sequence	Product size (bp)
ALP	Forward:5'- CTATCCTGGCTCCGTGCTC-3'	100
	Reverse:5'- GCTGGCAGTGGTCAGATGTT-3'	
OCN	Forward: 5'-CTCACACTCCTCGCCCTATT-3'	107
	Reverse:5'- TTGGACACAAAGGCTGCAC-3'	
BMP-2	Forward:5'-ACCCGCTGTCTTCTAGCGT-3'	180
	Reverse:5'-TTTCAGGCCGAACATGCTGAG-3'	
GAPDH	Forward:5'-TCAAGAAGGTGGTGAAGCAGG-3'	131
	Reverse:5'-GCGTCAAAGGTGGAGGAGTG-3'	
ALP, alkaline phosphatase; OCN, osteocalcin; BMP-2, bone morphogenetic protein-2.		

Surgical procedure

The hUC-MSCs were seeded onto 10 × 4 × 3 mm nHAC/PLA scaffolds in 24-well plates at a density of 1×10^7 cells/cm^2 per sample and were cultured in 1 ml mentioned above medium for 7 days. Next, the segmental jaw bone defects (10 × 4 × 3 mm) were performed in 24 6-month-old female New Zealand white rabbits (2.80 ± 0.35 kg; Medical Laboratory Animal Center of Chinese PLA General Hospital; Fig. 1). New Zealand white rabbits in each group were administered using 0.5 ml/kg 1:1(V/V) xylazine hydrochloride injection [catalog no. (2015)070011777; 0.25 mg/kg; HuaMu Animal Health Products Co., Ltd.; Jilin; China] and midazolam injection (catalog no. H10980025; 5 mg/kg; Jiangsu Nhwa Pharmaceutical Co., Ltd.; China) by intramuscular injection. And then the nHAC/PLA, hUC-MSCs +

nHAC/PLA, hUC-MSCs + nHAC/PLA + OMD, and hUC-MSCs + nHAC/PLA + OMD + rhBMP-7 were implanted into the jaw bone defects of 24 New Zealand white rabbits and subcutaneously into the backs of 6 6-week-old female nude mice (18.00 ± 0.26 g; Medical Laboratory Animal Center of Chinese PLA General Hospital). New Zealand white rabbits were housed in cages in a normal environment with a temperature of 16–26˚C, a relative humidity of 40–70%, a minimum air change of 8 times per h. The nude mice were housed in cages in a barrier environment with a temperature of 20–26˚C, a relative humidity of 40–70%, a minimum air change of 15 times per h. They were exposed to 12 h of light and 12 h of darkness every day and fed a regular diet and drinking water. All surgical procedures and care administered to the animals were approved by the Animal Care Committee of the People's Liberation Army General Hospital and performed according to their guidelines (ethics approval no. 2018-X14-87).

Assessment of bone formation

After 3 months of implantation, the rabbits were sacrificed by anesthesia;the nude mice were sacrificed by cervical dislocation. The implants of jaw bone defect and the back of nude mice were removed surgically, and then were fixed in 10% formalin. The implants of jaw bone defect were evaluated by the Quantum GX μCT System with a source voltage of 70 kV, current of 114 μA and 4.5 μm accuracy. Three-dimensional images of the defects were reconstructed from the scans by the Quantum GX μCT Workstation.

Next, all implants were embedded, specimens were trimmed using waterproof polishing paper without demineralization, cut into 5-μm sections, and stained using hematoxylin and eosin for 5 min at room temperature. The stained sections were photographed under an inverted light microscope. For morphometric analysis, the extent of newly formed bone was indicated by the percentage of bone formation area within the section. Every 5 sections, picked one, and then five consecutive sections per implant were obtained to evaluate the percentage of bone formation area. Five fields of view were selected for each section per implant under an inverted light microscope (magnification x200) and were calculated using a Leica Qwin v3.2 image analysis system (Leica Microsystems Inc.). Total scores per section were calculated and averaged for all sections to obtain an overall score for each implant. Data were then averaged across all implants within each group.

Furthermore, the sections of ectopic implants were examined by immunohistochemical staining. Simply, the sections were incubated using mouse anti-human OCN monoclonal antibody (catalog no. MAB1419; 1:50; R&D Systems, Inc.) overnight at 4˚C. The sections were then washed using PBS and incubated with biotin-conjugated swine-anti-mouse IgG (catalog no. Sp-9002; Beijing Zhongshan Goldenbridge Biotechnology Co., Ltd.) working solutions for 2 h at room temperature. Subsequently, the sections were washed using PBS and incubated with streptavidin-biotin complex/horseradish peroxidase working solutions (catalog nos. SP-9002; Beijing Zhongshan Goldenbridge Biotechnology Co., Ltd.) for 1 h at room temperature. Next, the staining was visualized by using 3,3'-diaminobenzidine (catalog no. zli-9018; Beijing Zhongshan Goldenbridge Biotechnology Co., Ltd.), and then the sections were stained with hematoxylin dye solution for 5 min at room temperature. Negative controls were incubated with PBS instead of primary antibody. The stained sections were photographed under an inverted light microscope.

Statistical analysis

All data are presented as the mean ± standard deviation. Statistical analysis was performed using SPSS 13.0 (SPSS, Inc.). Levene's test was used to verify the homogeneity of variance of data. Statistical significance was assessed using one-way analysis of variance and Tukey's multiple comparison tests. Tamhane's T2 multiple comparison test was used on data with a non-normal distribution or unequal variance. $P < 0.05$ was considered to indicate a statistically significant difference.

Results

Culture, proliferation, phenotype and multilineage differentiation potential of hUC-MSCs

The Wharton's Jelly was isolated from umbilical cord tissues (Fig. 2A). The cells migrated from fragments of Wharton's Jelly after 3–4 days of culture (Fig. 2B). The phase 3 hUC-MSCs exhibited typical fibroblastic morphology on day 1 of culture (Fig. 2C), and were arranged in a radial or whirlpool arrangement on day 4 of culture (Fig. 2D). In the first 3 days of the incubation period, the cells did not markedly proliferate, and they entered the logarithmic growth period on days 4–7. Cell proliferation reached the highest point on day 8 and entered the platform stage (Fig. 2E). The cells expressed The cells expressed CD73 (99.78%), CD90 (99.89%) and CD105 (99.72%), and did not express CD11a (0.08%), CD45 (0.32%), CD34 (2.31%) and human leukocyte antigen HLA-DR (0.09%; Fig. 2F). Under specific culture conditions, the cells differentiated into osteogenic (Fig. 2G) and adipogenic (Fig. 2H) lineages.

Effect of rhBMP-7 on the osteogenic differentiation of hUC-MSCs seeded on culture plates

When cultured in OMD and OMD + rhBMP-7 for 14 days, the hUC-MSCs were positively stained for OCN (Fig. 3), ALP (Fig. 4A), and a large number of mineralized substrates were produced (Fig. 4B). The exogenously-added rhBMP-7 resulted in more intensive alkaline phosphatase and Alizarin red staining. The mineral formation measurements demonstrated that the hUC-MSCs + OMD ($P < 0.001$) and hUC-MSCs + OMD + rhBMP-7 ($P < 0.001$) groups had a significantly higher mineral formation compared with that of the hUC-MSCs group. In addition, the hUC-MSCs + OMD group had a significantly lower mineral formation compared with that of the hUC-MSCs + OMD + rhBMP-7 group ($P < 0.05$; Fig. 4C).

Effect of rhBMP-7 on the proliferation of hUC-MSCs combined with nHAC/PLA

NHAC/PLA exhibited a nano-to-microscale hierarchical architecture of natural, cancellous bones (Fig. 4D) by scanning electron microscopy. When cultured in serum-free medium for 7 days, the cells adhered, extended and proliferated on the surface and in the pore of the nHAC/PLA, and produced some filarious extracellular matrixes (Fig. 4E). When cultured in serum-free OMD without (Fig. 4F) or with (Fig. 4G) rhBMP-7, the cells were covered by abundant amounts of matrix protein deposits.

Cell proliferation in the hUC-MSCs + nHAC/PLA, hUC-MSCs + nHAC/PLA + OMD, and hUC-MSCs + nHAC/PLA + OMD + rhBMP-7 groups reached the highest points on days 9, 5 and 7, respectively. This value in the hUC-MSCs + nHAC/PLA + OMD ($P < 0.01$) and hUC-MSCs + nHAC/PLA + OMD + rhBMP-7 ($P < 0.01$) groups was significantly higher compared with that of the hUC-MSCs + nHAC/PLA group on day 1.

Cell proliferation in the hUC-MSCs + nHAC/PLA + OMD and hUC-MSCs + nHAC/PLA + OMD + rhBMP-7 groups was significantly lower compared with that of the hUC-MSCs + nHAC/PLA group on days 5 ($P < 0.01$ and $P < 0.05$, respectively), 7 ($P < 0.001$ and $P < 0.001$, respectively) and 9 ($P < 0.001$ and $P < 0.001$, respectively). This value in the hUC-MSCs + nHAC/PLA + OMD group was significantly lower compared with that in the hUC-MSCs + nHAC/PLA + OMD + rhBMP-7 group on days 7 ($P < 0.01$) and 9 ($P < 0.01$; Fig. 5A).

Effect of rhBMP-7 on the osteogenic differentiation of hUC-MSCs combined with nHAC/PLA

The hUC-MSCs + nHAC/PLA + OMD and hUC-MSCs + nHAC/PLA + OMD + rhBMP-7 groups had a significantly higher Ca concentration ($P < 0.001$), P concentration ($P < 0.001$), ALP activity ($P < 0.05$) and OCN concentration ($P < 0.01$) compared with those of the hUC-MSCs + nHAC/PLA group on days 7 and 14. The hUC-MSCs + nHAC/PLA + OMD + rhBMP-7 group had a significantly higher P ($P < 0.01$) and OCN concentration ($P < 0.05$) compared with the hUC-MSCs + nHAC/PLA + OMD group on day 7. The hUC-MSCs + nHAC/PLA + OMD + rhBMP-7 group had a significantly higher Ca concentration ($P < 0.01$), P concentration ($P < 0.05$), ALP activity ($P < 0.05$) and OCN concentration ($P < 0.01$) compared with the hUC-MSCs + nHAC/PLA + OMD group on day 14 (Fig. 5B-E).

The constructs induced for 14 days were stained with alizarin red and photographed (Fig. 6A). The hUC-MSCs + nHAC/PLA + OMD ($P < 0.001$) and hUC-MSCs + nHAC/PLA + OMD + rhBMP-7 ($P < 0.001$) groups had a significantly higher mineral formation compared with that of the hUC-MSCs + nHAC/PLA group. In addition, the hUC-MSCs + nHAC/PLA + OMD group had a significantly lower mineral formation compared with that of the hUC-MSCs + nHAC/PLA + OMD + rhBMP-7 group ($P < 0.01$; Fig. 6B).

The hUC-MSCs + nHAC/PLA + OMD and hUC-MSCs + nHAC/PLA + OMD + rhBMP-7 groups had significantly higher ALP ($P < 0.001$), OCN ($P < 0.001$) and BMP-2 ($P < 0.01$) mRNA expression levels compared with the hUC-MSCs + nHAC/PLA group on days 7 and 14. The hUC-MSCs + nHAC/PLA + OMD group had significantly lower ALP ($P < 0.05$), OCN ($P < 0.001$) and BMP-2 ($P < 0.001$,) mRNA expression levels compared with the hUC-MSCs + nHAC/PLA + OMD + rhBMP-7 group on days 7 and 14 (Fig. 6C-E).

Effect of rhBMP-7 on bone formation of the jaw bone defect and the back of nude mice using hUC-MSCs combined with nHAC/PLA

When the constructs were implanted into jaw bone defects for 3 months, the newly formed mineralized tissue covering the defect could be observed in all groups by three-dimensional micro-CT reconstruction (Fig. 7). Hematoxylin and eosin staining showed that the nHAC/PLA (Fig. 7A), hUC-MSCs + nHAC/PLA (Fig. 7B), hUC-MSCs + nHAC/PLA + OMD (Fig. 7C) and hUC-MSCs + nHAC/PLA + OMD + rhBMP-7 (Fig. 7D) groups exhibited obvious new bone formation. The new bone edges were arranged in a spindle morphology osteoblasts, and the newly formed bones had new blood vessels passing through.

When the constructs were implanted into the back of nude mice for 3 months, hematoxylin and eosin staining showed that the nHAC/PLA (Fig. 7A) and hUC-MSCs + nHAC/PLA (Fig. 7B) groups had no bone formation, with a few blood vessels and a large number of residual nHAC/PLA following degradation.

The hUC-MSCs + nHAC/PLA + OMD (Fig. 7C) and hUC-MSCs + nHAC/PLA + OMD + rhBMP-7 (Fig. 7D) groups exhibited new bone formation, abundant blood vessels and active osteoblasts.

In bone formation of the jaw bone defect, the morphometric analysis demonstrated that the percentage of the bone formation area in the hUC-MSCs + nHAC/PLA ($P < 0.001$), hUC-MSCs + nHAC/PLA + OMD ($P < 0.001$) and hUC-MSCs + nHAC/PLA + OMD + rhBMP-7 ($P < 0.001$) groups was significantly higher than that in the nHAC/PLA group. The percentage of bone formation area in the hUC-MSCs + nHAC/PLA + OMD ($P < 0.001$) and the hUC-MSCs + nHAC/PLA + OMD + rhBMP-7 ($P < 0.001$) groups was significantly higher than that in the hUC-MSCs + nHAC/PLA group. But, the percentage of bone formation area in the hUC-MSCs + nHAC/PLA + OMD was significantly lower than that in hUC-MSCs + nHAC/PLA + OMD + rhBMP-7 group ($P < 0.01$; Fig. 8).

In bone formation of the back of nude mice, the morphometric analysis demonstrated that the percentage of bone formation area in the hUC-MSCs + nHAC/PLA + OMD and hUC-MSCs + nHAC/PLA + OMD + rhBMP-7 groups was significantly higher compared with that in the hUC-MSCs + nHAC/PLA ($P < 0.001$) and nHAC/PLA ($P < 0.001$) groups. No significant difference was identified between the hUC-MSCs + nHAC/PLA and nHAC/PLA groups. However, the percentage of bone formation area in the hUC-MSCs + nHAC/PLA + OMD + rhBMP-7 group was significantly higher compared with that in the hUC-MSCs + nHAC/PLA + OMD group ($P < 0.01$; Fig. 8). Furthermore, in the same group, bone formation in jaw bone defect was significantly higher than that in the back of nude mice ($P < 0.001$; Fig. 8). The contribution of implanted hUC-MSCs to new bone formation in the back of nude mice was detected by immunohistochemical staining of anti-human OCN monoclonal antibodies. The nHAC/PLA (Fig. 9A) and hUC-MSCs + nHAC/PLA (Fig. 9B) groups did not express OCN; but hUC-MSCs + nHAC/PLA + OMD (Fig. 9C) and hUC-MSCs + nHAC/PLA + OMD + rhBMP-7 (Fig. 9D) groups positively expressed OCN and; the expression of OCN was negative when PBS was used instead of the primary antibody (Fig. 9E).

Discussion

In this study, the isolated cells exhibited typical fibroblastic morphology; they expressed MSC markers, did not express hematopoietic stem cell markers and HLA-DR surface molecules, and exhibited self-renewal and multilineage differentiation potential. These results suggested that our cultured cells were mesenchymal stem cells [43].

When these cells were seeded on nHAC/PLA and cultured in human MSC serum-free OMD with or without rhBMP-7, except for the initial stress response (day 1) and adaptive phase (day 3), both OMD and OMD + rhBMP-7 inhibited cell proliferation. OMD, including dexamethasone, ascorbic acid and β-glycerophosphate, is routinely used for the osteogenic differentiation of MSCs. Certain reports have shown that high concentrations of dexamethasone inhibit the proliferation of hBM-MSCs by disrupting mitochondrial dynamics [44]; and the accumulation of ascorbic acid-produced type I collagen partly leads to the cessation of cell proliferation [45]. In addition, a study demonstrated that BMP-7 down-regulated the genes associated with cell cycle regulation, attenuating cell cycle progression and cell proliferation

during early osteogenic differentiation of human MSCs [46]. Our results were consistent with these studies, showing that OMD and OMD + rhBMP-7 inhibited cell proliferation. However, the culture with OMD + rhBMP-7 exhibited a higher cell proliferation compared with that with OMD, indicating that the addition of rhBMP-7 attenuated the inhibitory effect of OMD on cell proliferation; the relevant mechanisms needed to be further explored.

When these cells were seeded on culture plate and cultured in human MSC serum-free OMD with or without rhBMP-7, as the cultures progressed, the cells positively expressed OCN, became alkaline phosphatase and mineral formation positive histochemically; when these cells were seeded on nHAC/PLA, the Ca concentration, P concentration, ALP activity, OCN concentration, mineral formation, and the mRNA expression levels of ALP, OCN and BMP-2 were also up-regulated by OMD and OMD + rhBMP-7. ALP is considered one of the earliest phenotypic markers of osteogenic differentiation [45]. That ALP mRNA and ALP activity were increased indicated the begin of osteogenic differentiation of hUC-MSCs. Meantime, OCN is a bone-specific protein synthesized by osteoblasts that represents a late marker of osteogenic differentiation, and is associated with the mineralized matrix [45]. OCN mRNA and OCN secretion were up-regulated indicated that the mineralization of hUC-MSCs progressed. These results suggested that both OMD and OMD + rhBMP-7 could promote osteogenic differentiation of hUC-MSCs in two or three-dimensional culture. Furthermore, the exogenously-added rhBMP-7 enhanced the promoting effect of OMD on osteogenic differentiation of hUC-MSCs; the higher BMP-2 mRNA expression level indicated that the endogenously-produced BMPs might serve an important regulatory role in the process. The previous study demonstrated that the addition of rhBMP-7 enhanced osteogenic differentiation of murine MSCs and produced a reciprocal expression profile in the expression of endogenous BMPs, as compared with BMP antagonism. Osteogenic differentiation is regulated by a complex network of multiple BMPs that exhibit selective increases and decreases in expression during differentiation [46]. The transient knockdown of BMP-2 using small interfering RNA demonstrated that the osteoinductive properties of BMP-7 are independent of endogenous BMP-2 expression in human MSCs [46]. BMP-7 has been also reported to induce BMP-2 expression in murine MSCs [36]. In short, the mechanism of the effect of rhBMP-7 on the proliferation and osteogenic differentiation of human or animal MSCs is currently controversial, but the fact that osteogenic differentiation is regulated by a complex network of multiple BMPs is fundamentally accepted.

Stem cells, scaffold and osteogenic factor are three main factors for creating a stem cell-based tissue-engineered bone. They form the microenvironment in which cells grow *in vitro*. The nHAC/PLA provides a three-dimensional space for hUC-MSC adhesion, proliferation and differentiation [40]. A previous study confirmed that bioactive ceramic coatings depend on its interfacial dissolution, precipitation and ion exchange reactions to affect cellular proliferation, differentiation, collagen deposition and mineralization [47]. The continuous deposition of hydroxyapatite in the extracellular matrix is known as biomineralization. This extension of hydroxyapatite requires appropriate Ca^{2+} and PO^{3-}_4 concentrations outside the extracellular matrix [48]. Therefore, the culture medium outside the constructs needs to have sufficient Ca^{2+} and PO^{3-}_4 to support the continuous formation of new hydroxyapatite. In the present

study, the nHAC/PLA contained 45 ± 5% hydroxyapatite, and when the constructs were cultured in serum-free OMD medium, the microenvironment of the medium was changed by the attachment, proliferation, differentiation and secretions of hUC-MSCs, leading the nHAC/PLA to process physical and chemical dissolution. Therefore, Ca and P concentration in the medium increased to form more hydroxyapatite for mineralization of hUC-MSCs. In addition, the exogenously-added rhBMP-7 significantly enhanced osteogenic differentiation in hUC-MSCs combined with nHAC/PLA, which caused hUC-MSCs to produce more matrix proteins, such as ALP and OCN, as determined by the Roche kits and real-time polymerase chain reaction assay, and further promoted the degradation of nHAC/PLA, which provided more Ca^{2+} and PO^{-3}_4 to form the hydroxyapatite needed for hUC-MSC mineralization. In conclusion, the resulting hUC-MSCs + nHAC/PLA + OMD + rhBMP-7 construct exhibited an abundantly mineralized matrix containing differentiated osteoblasts, as determined by Alizarin Red staining. The microenvironment formed by nHAC/PLA, OMD, rhBMP-7 and hUC-MSCs led to a successful cell proliferation, differentiation, and mineralization in the constructs.

In vivo studies on the bone formation ability of hUC-MSCs in oral maxillo-facial bone defect are rare, to the best of our knowledge. Of note, when the sterile, resorbable 10 × 4 × 3 mm nHAC/PLA scaffolds with or without 1×10^7 cell/cm^2 and osteoinductive factor cultured *in vitro* for 7 days were transplanted subcutaneously into the back of nude mice for heterotopic bone formation and transplanted into jaw bone defect for jaw bone bone formation, both nHAC/PLA and hUC-MSCs + nHAC/PLA exhibited bone formation in jaw bone defect, but not in the back of nude mice. A previous study verified that the pore size of scaffolds needed for bone ingrowth is ≥ 100 μm, and the most favorable pore size for new bone formation is 300–400 μm [49]. In the present study, the porosities of nHAC/PLA were 70–88%, and the pore sizes were 300 ± 250 μm; the favorable interconnected pores promoted the diffusion of oxygen and nutrients into nHAC/PLA in the jaw bone defect microenvironment, and made native host cells migrate into materials and proliferate, differentiate, produce blood vessels and finally form new bone within the porous structures. The recruited native host cells from the jaw bone defect microenvironment may be responsible for the subsequent bone formation and remodeling. Therefore, the jaw bone defect microenvironment served an important role in the bone formation of nHAC/PLA itself. Furthermore, the hUC-MSCs + nHAC/PLA group exhibited a significantly higher percentage of bone formation area compared with the nHAC/PLA group. A previous study reported that hUC-MSCs, human-induced pluripotent stem cells and hBM-MSCs exhibit a significantly larger amount of new bone compared with a cell-free macroporous calcium phosphate cement control in rat cranial defects [50]. This indicated that an *in vivo* bone defect microenvironment is also an important factor in bone tissue engineering, which provides signals to promote *in vitro* uninduced-MSCs differentiate into osteoblasts to participate in the process of bone regeneration. Both the hUC-MSCs + nHAC/PLA + OMD and hUC-MSCs + nHAC/PLA + OMD + rhBMP-7 groups exhibited bone formation in the back of nude mice and jaw bone defect, the higher bone formations were presented in hUC-MSCs + nHAC/PLA + OMD + rhBMP-7 group and in jaw bone defect. And the contribution of implanted hUC-MSCs to new bone formation was detected by immunohistochemical staining of anti-human OCN monoclonal antibodies. It further demonstrated that exogenously-added rhBMP-7 enhanced bone formatiom ability of hUC-MSCs; rhBMP-7 and *in situ* bone

defect microenvironment may provide a more optimized microenvironment for bone regeneration in hUC-MSCs combined with nHAC/PLA.

Conclusion

The hUC-MSCs + nHAC/PLA + OMD + rhBMP-7 enhanced jaw bone regeneration. That the microenvironment formed by the regenerative engineered constructs and an *in situ* bone defect microenvironment closely matched that of the bone tissue in its native state may be essential for sufficient and timely bone regeneration. This hUC-MSCs-based construct is a better alternative for clinical jaw bone regenerative therapeutic applications.

Abbreviations

hUC-MSCs: Human umbilical cord mesenchymal stem cells; rhBMP-7: Recombinant human bone morphogenetic protein-7; nHAC/PLA: Nano-hydroxyapatite/collagen/poly(L-lactide); ALP: Alkaline phosphatase; OCN: Osteocalcin; BMP: Bone morphogenetic protein; OMD: Osteogenic media; hBM-MSCs: Human bone marrow-derived mesenchymal stem cells; hESCs: Human embryonic stem cells; FDA: Food and Drug Administration; BMPs: Bone morphogenetic proteins; PLA: People's Liberation Army; Ca: Calcium; P: phosphorous

Declarations

Acknowledgments

Not applicable

Funding

This work was supported by Clinical Research Fostering Fund of Chinese PLA General Hospital (2016FC-CXYY-2007, 2015FC-CXYY-1003), National Natural Science Fund (81271180), Special Grade of the Financial Support from the China Postdoctoral Science Foundation (2020T130744) and Postdoctoral Science Foundation of China (2018M643873).

Availability of data and materials

The datasets used and/or analysed during the current study are available from the corresponding author on reasonable request.

Authors' contributions

All authors read and approved the final manuscript. Ling-ling E contributed to design, collection and assembly of data, data analysis and interpretation, and manuscript writing. Helin Xing, Xing Wang and Tao Cheng contributed to revision and final approval of the manuscript. Shou Zhang and Xiaocao Ma

contributed to review and editing of the manuscript. Rong Zhang and Hongchen Liu contributed to conception, financial support and revision and final approval of the manuscript.

Ethics approval and consent to participate

This study was approved by the committee of experimentation of Chinese PLA General Hospital.

Consent for publication

Not applicable.

Competing interests

The authors declare that they have no competing interests.

References

1. Brauner E, Jamshir S, Guarino G, Ciolfi A, Valentini V, Pompa G, Di Carlo S. Pleomorphic Adenoma Rehabilitative Treatment in Growing Up Patient: A 20-years Follow-Up. Eur Rev Med Pharmacol Sci. 2016;20(17):3523-7.
2. Oryan A, Alidadi S, Moshiri A, Maffulli N. Bone Regenerative Medicine: Classic Options, Novel Strategies, and Future Directions. J Orthop Surg Res. 2014;9(1):18.
3. Pilipchuk SP, Plonka AB, Monje A, Taut AD, Lanis A, Kang B, Giannobile WV. Tissue engineering for bone regeneration and osseointegration in the oral cavity. Dent Mater. 2015;31(4):317-38.
4. Cao Y, Gang X, Sun C, Wang G. Mesenchymal Stem Cells Improve Healing of Diabetic Foot Ulcer. J Diabetes Res. 2017;2017:9328347.
5. Kretlow JD, Young S, Klouda L, Wong M, Mikos AG. Injectable biomaterials for regenerating complex craniofacial tissues. Adv Mater. 2009;21(32-33):3368-93.
6. Mikos AG, Herring SW, Ochareon P, Elisseeff J, Lu HH, Kandel R, Schoen FJ, Toner M, Mooney D, Atala A, et al. Engineering complex tissues. Tissue Eng. 2006;12(12):3307-39.
7. Kong HJ, Smith MK, Mooney DJ. Designing alginate hydrogels to maintain viability of immobilized cells. Biomaterials. 2003;24(22):4023-9.
8. Crisan M, Yap S, Casteilla L, Chen CW, Corselli M, Park TS, Andriolo G, Sun B, Zheng B, Zhang L, et al. A perivascular origin for mesenchymal stem cells in multiple human organs. Cell Stem Cell. 2008;3(3):301-13.
9. Arutyunyan I, Elchaninov A, Makarov A, Fatkhudinov T. Umbilical Cord as Prospective Source for Mesenchymal Stem Cell-Based Therapy. Stem Cells Int. 2016;2016:6901286.
10. Can A, Karahuseyinoglu S. Concise review: human umbilical cord stroma with regard to the source of fetus-derived stem cells. Stem Cells. 2007;25(11):2886-95.

11. Nekanti U, Rao VB, Bahirvani AG, Jan M, Totey S, Ta M. Long-term expansion and pluripotent marker array analysis of Wharton's jelly-derived mesenchymal stem cells. Stem Cells Dev. 2010;19(1):117-30.
12. Han Y, Chai J, Sun T, Li D, Tao R. Differentiation of human umbilical cord mesenchymal stem cells into dermal fibroblasts in vitro. Biochem Biophys Res Commun. 2011;413(4):561-5.
13. Wang XY, Lan Y, He WY, Zhang L, Yao HY, Hou CM, Tong Y, Liu YL, Yang G, Liu XD, et al. Identification of mesenchymal stem cells in aorta-gonad-mesonephros and yolk sac of human embryos. Blood. 2008;111(4):2436-43.
14. Fong CY, Chak LL, Biswas A, Tan JH, Gauthaman K, Chan WK, Bongso A. Human Wharton's jelly stem cells have unique transcriptome profiles compared to human embryonic stem cells and other mesenchymal stem cells. Stem Cell Rev Rep. 2011;7(1):1-16.
15. Gauthaman K, Fong CY, Suganya CA, Subramanian A, Biswas A, Choolani M, Bongso A. Extra-embryonic human Wharton's jelly stem cells do not induce tumorigenesis, unlike human embryonic stem cells. Reprod Biomed Online. 2012;24(2):235-46.
16. Subramanian A, Shu-Uin G, Kae-Siang N, Gauthaman K, Biswas A, Choolani M, Bongso A, Chui-Yee F. Human umbilical cord Wharton's jelly mesenchymal stem cells do not transform to tumor-associated fibroblasts in the presence of breast and ovarian cancer cells unlike bone marrow mesenchymal stem cells. J Cell Biochem. 2012;113(6):1886-95.
17. Weiss ML, Medicetty S, Bledsoe AR, Rachakatla RS, Choi M, Merchav S, Luo Y, Rao MS, Velagaleti G, Troyer D. Human umbilical cord matrix stem cells: preliminary characterization and effect of transplantation in a rodent model of Parkinson's disease. Stem Cells Stem Cells. 2006;24(3):781-92.
18. Goyal U, Sen A, Ta M. Isolation and Molecular Characterization of Progenitor Cells from Human Umbilical Cord. Methods Mol Biol. 2019;2029:1-13.
19. Sarugaser R, Lickorish D, Baksh D, Hosseini MM, Davies JE. Human umbilical cord perivascular (HUCPV) cells: a source of mesenchymal progenitors. Stem Cells. 2005;23(2):220-9.
20. Borys-Wójcik S, Brązert M, Jankowski M, Ożegowska K, Chermuła B, Piotrowska-Kempisty H, Bukowska D, Antosik P, Pawelczyk L, Nowicki M, et al. Human Wharton's jelly mesenchymal stem cells: properties, isolation and clinical applications. J Biol Regul Homeost Agents. 2019;33(1):119-23.
21. Zhang H, Tao Y, Ren S, Liu H, Zhou H, Hu J, Tang Y, Zhang B, Chen H. Simultaneous harvesting of endothelial progenitor cells and mesenchymal stem cells from the human umbilical cord. Exp Ther Med. 2018;15(1):806-12.
22. Dos Santos A, Balayan A, Funderburgh ML, Ngo J, Funderburgh JL, Deng SX. Differentiation Capacity of Human Mesenchymal Stem Cells into Keratocyte Lineage. Invest Ophthalmol Vis Sci. 2019;60(8):3013-23.
23. Karahuseyinoglu S, Kocaefe C, Balci D, Erdemli E, Can A. Functional structure of adipocytes differentiated from human umbilical cord stroma-derived stem cells. Stem Cells. 2008;26(3):682-91.
24. Van Pham P, Truong NC, Le PT, Tran TD, Vu NB, Bui KH, Phan NK. Isolation and proliferation of umbilical cord tissue derived mesenchymal stem cells for clinical applications. Cell Tissue Bank.

2016;17(2):289-302.
25. Li X, Bai J, Ji X, Li R, Xuan Y, Wang Y. Comprehensive characterization of four different populations of human mesenchymal stem cells as regards their immune properties, proliferation and differentiation. Int J Mol Med. 2014;34(3):695-704.
26. Chen MY, Lie PC, Li ZL, Wei X. Endothelial differentiation of Wharton's jelly-derived mesenchymal stem cells in comparison with bone marrow-derived mesenchymal stem cells. Exp Hematol. 2009;37(5):629-40.
27. Wu LF, Wang NN, Liu YS, Wei X. Differentiation of Wharton's jelly primitive stromal cells into insulin-producing cells in comparison with bone marrow mesenchymal stem cells. Tissue Eng Part A. 2009;15(10):2865-73.
28. Lu LL, Liu YJ, Yang SG, Zhao QJ, Wang X, Gong W, Han ZB, Xu ZS, Lu YX, Liu D, et al. Isolation and characterization of human umbilical cord mesenchymal stem cells with hematopoiesis-supportive function and other potentials. Haematologica. 2006;91(8):1017-26.
29. Shaer A, Azarpira N, Aghdaie MH, Esfandiari E. Isolation and characterization of Human Mesenchymal Stromal Cells Derived from Placental Decidua Basalis; Umbilical cord Wharton's Jelly and Amniotic Membrane. Pak J Med Sci. 2014;30(5):1022-6.
30. Tseng SS, Lee MA, Reddi AH. Nonunions and the potential of stem cells in fracture-healing. J Bone Joint Surg Am. 2008;90 Suppl 1:92-8.
31. Cho TJ, Gerstenfeld LC, Einhorn TA. Differential temporal expression of members of the transforming growth factor beta superfamily during murine fracture healing. J Bone Miner Res. 2002;17(3):513-20.
32. Lyons KM, Hogan BL, Robertson EJ. Colocalization of BMP 7 and BMP 2 RNAs suggests that these factors cooperatively mediate tissue interactions during murine development. Mech Dev. 1995;50(1):71-83.
33. Cook SD, Wolfe MW, Salkeld SL, Rueger DC. Effect of recombinant human osteogenic protein-1 on healing of segmental defects in non-human primates. J Bone Joint Surg Am. 1995;77(5):734-50.
34. Kanakaris NK, Giannoudis PV. Clinical applications of bone morphogenetic proteins: current evidence. J Surg Orthop Adv. 2008;17(3):133-46.
35. Knippenberg M, Helder MN, Zandieh Doulabi B, Wuisman PI, Klein-Nulend J. Osteogenesis versus chondrogenesis by BMP-2 and BMP-7 in adipose stem cells. Biochem Biophys Res Commun. 2006;342(3):902-8.
36. Edgar CM, Chakravarthy V, Barnes G, Kakar S, Gerstenfeld LC, Einhorn TA. Autogenous regulation of a network of bone morphogenetic proteins (BMPs) mediates the osteogenic differentiation in murine marrow stromal cells. Bone. 2007;40(5):1389-98.
37. Liao SS, Cui FZ, Zhang W, Feng QL. Hierarchically biomimetic bone scaffold materials: nano-HA/collagen/PLA composite. J Biomed Mater Res B Appl Biomater. 2004;69(2):158-65.
38. Liao S, Wang W, Uo M, Ohkawa S, Akasaka T, Tamura K, Cui F, Watari F. A three-layered nano-carbonated hydroxyapatite/collagen/PLGA composite membrane for guided tissue regeneration. Biomaterials. 2005;26(36):7564-71.

39. He H, Yu J, Cao J, E L, Wang D, Zhang H, Liu H. Biocompatibility and Osteogenic Capacity of Periodontal Ligament Stem Cells on nHAC/PLA and HA/TCP Scaffolds. J Biomater Sci Polym Ed. 2011;22(1-3):179-94.
40. Liu HC, E LL, Wang DS, Su F, Wu X, Shi ZP, Lv Y, Wang JZ. Reconstruction of alveolar bone defects using bone morphogenetic protein 2 mediated rabbit dental pulp stem cells seeded on nano-hydroxyapatite/collagen/poly(L-lactide). Tissue Eng Part A Tissue Eng Part A. 2011;17(19-20):2417-33.
41. Mori Y, Ohshimo J, Shimazu T, He H, Takahashi A, Yamamoto Y, Tsunoda H, Tojo A, Nagamura-Inoue T. Improved explant method to isolate umbilical cord-derived mesenchymal stem cells and their immunosuppressive properties. Tissue Eng Part C Methods. 2015;21(4):367-72.
42. Livak and Schmittgen. Analysis of relative gene expression data using real-time quantitative PCR and the 2-ΔΔCt method. Methods. 2001;25: 402-8.
43. Dominici M, Le Blanc K, Mueller I, Slaper-Cortenbach I, Marini F, Krause D, Deans R, Keating A, Prockop Dj, Horwitz E. Minimal criteria for defning multipotent mesenchymal stromal cells. TeInternational Society for Cellular Terapy position statement. Cytotherapy. 2006;8(4):315-7.
44. Ma L, Feng X, Wang K, Song Y, Luo R, Yang C. Dexamethasone promotes mesenchymal stem cell apoptosis and inhibits osteogenesis by disrupting mitochondrial dynamics. FEBS Open Bio. 2019;10(2):211-20.
45. Lian JB, Stein GS. Development of the osteoblast phenotype: molecular mechanisms mediating osteoblast growth and differentiation. Iowa Orthop J. 1995;15:118-40.
46. Lavery K, Hawley S, Swain P, Rooney R, Falb D, Alaoui-Ismaili MH. New insights into BMP-7 mediated osteoblastic differentiation of primary human mesenchymal stem cells. Bone. 2009;45(1):27-41.
47. Manochantr S, U-pratya Y, Kheolamai P, Rojphisan S, Chayosumrit M, Tantrawatpan C, Supokawej A, Issaragrisil S. Immunosuppressive properties of mesenchymal stromal cells derived from amnion, placenta, Wharton's jelly and umbilical cord. Intern Med J Intern Med J. 2013;43(4):430-9.
48. 48. Ducheyne P, Cuckler JM. Bioactive ceramic prosthetic coatings. Clin Orthop Relat Res. 1992; (276):102-14.
49. Tsuruga E, Takita H, Itoh H, Wakisaka Y, Kuboki Y. Poresize of poroushydroxyapatite as the cell-substratumcontrolsBMP-inducedosteogenesis. J Biochem. 1997;121(2):317-24.
50. Wang P, Liu X, Zhao L, Weir MD, Sun J, Chen W, Man Y, Xu HH. Bone tissue engineering via human induced pluripotent, umbilical cord and bone marrow mesenchymal stem cells in rat cranium. Acta Biomater. 2015;18:236-48.

Figures

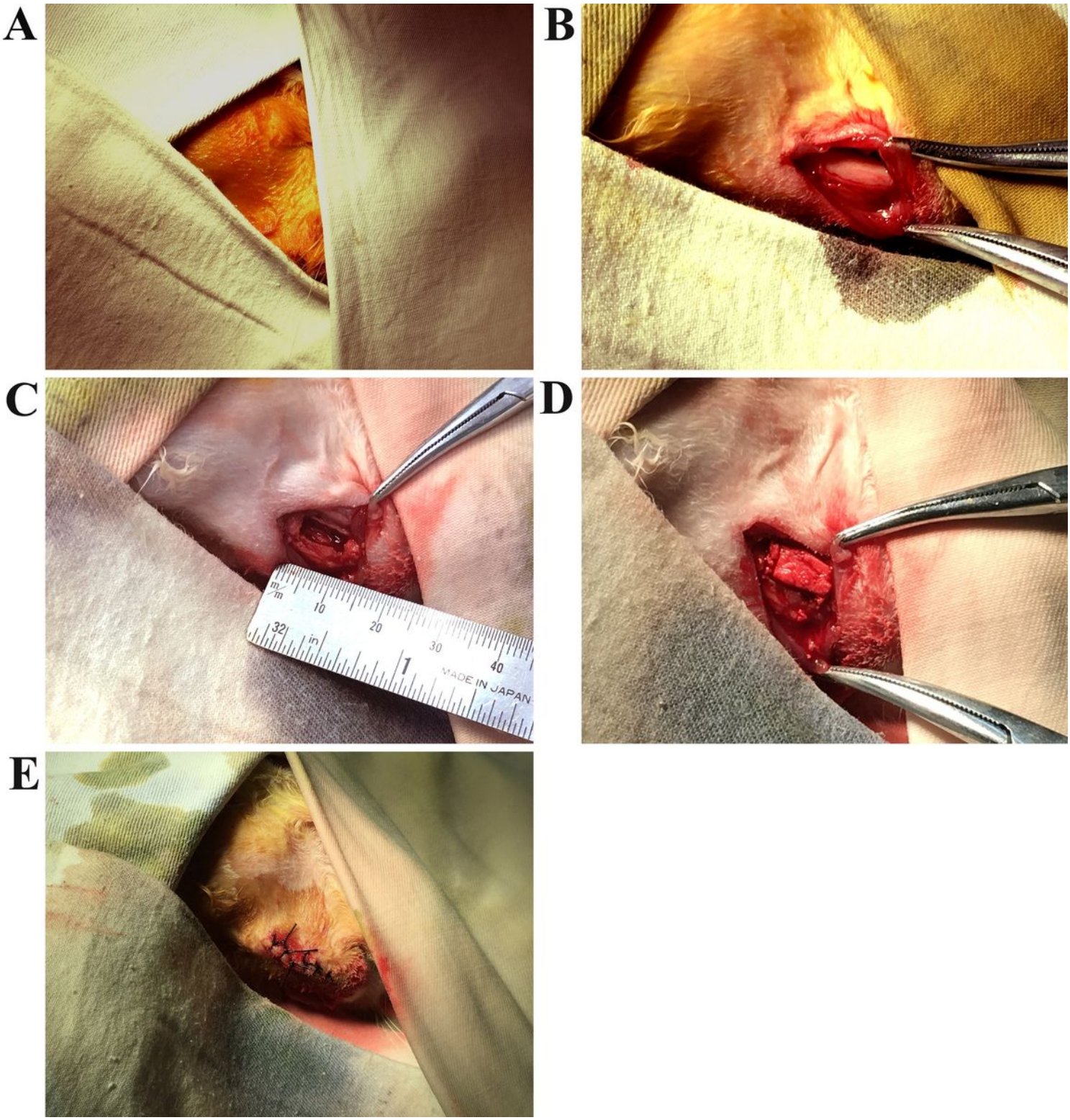

Figure 1

Surgical procedure. A Iodophor disinfection operation area and paved sterile disinfection outside the operation area. B Exposed rabbit mandible frontiers. C A 10x4x3 mm jaw bone defect. D Implantation of the hUC-MSCs+nHAC/PLA construct. E Suture incision. hUC-MSCs human umbilical cord mesenchymal stem cells, nHAC/PLA nano-hydroxyapatite/collagen/poly(L-lactide)

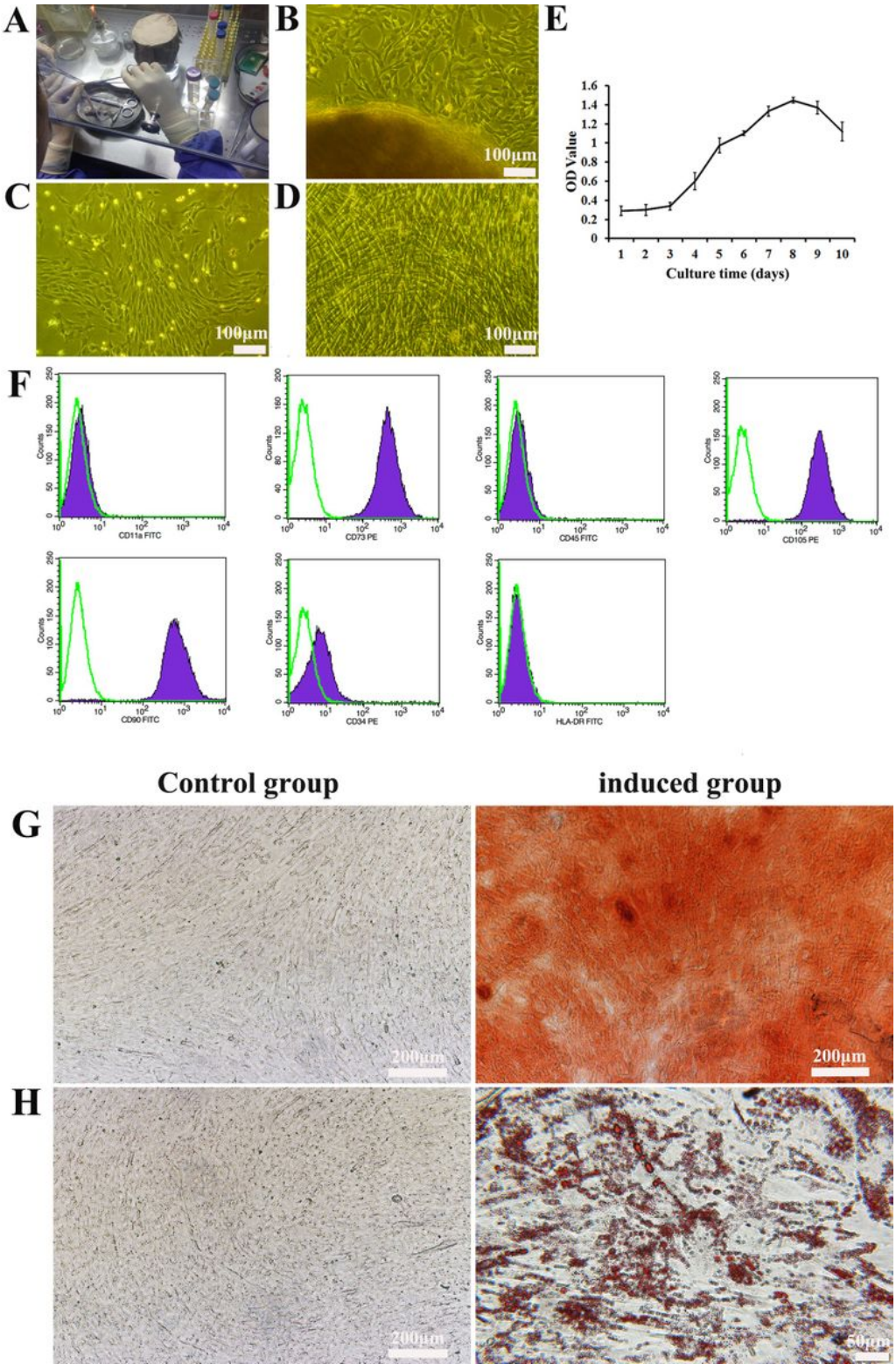

Figure 2

Characteristics of hUC-MSCs. A Umbilical cord. B Tissue explant culture of hUC-MSCs (scale bar=100 μm). C Phase 3 hUC-MSCs on day 1 of culture (scale bar=100 μm). D Phase 3 hUC-MSCs on day 4 of culture (scale bar=100 μm). E Proliferation of hUC-MSCs was evaluated using a Cell Counting Kit-8 assay. Data are presented as mean ± SD (n=12). F Phenotype of hUC-MSCs. Green line indicates isotype control, purple-shaded histograms indicate positive staining. G hUC-MSCs were induced into osteoblasts on day

21 of culture (scale bar=200 μm). H hUC-MSCs were induced into adipocytes on day 21 of culture (Control group scale bar=200 μm, induced group scale bar=50 μm). hUC-MSCs human umbilical cord mesenchymal stem cells, PE phycoerythrin, OD optical density

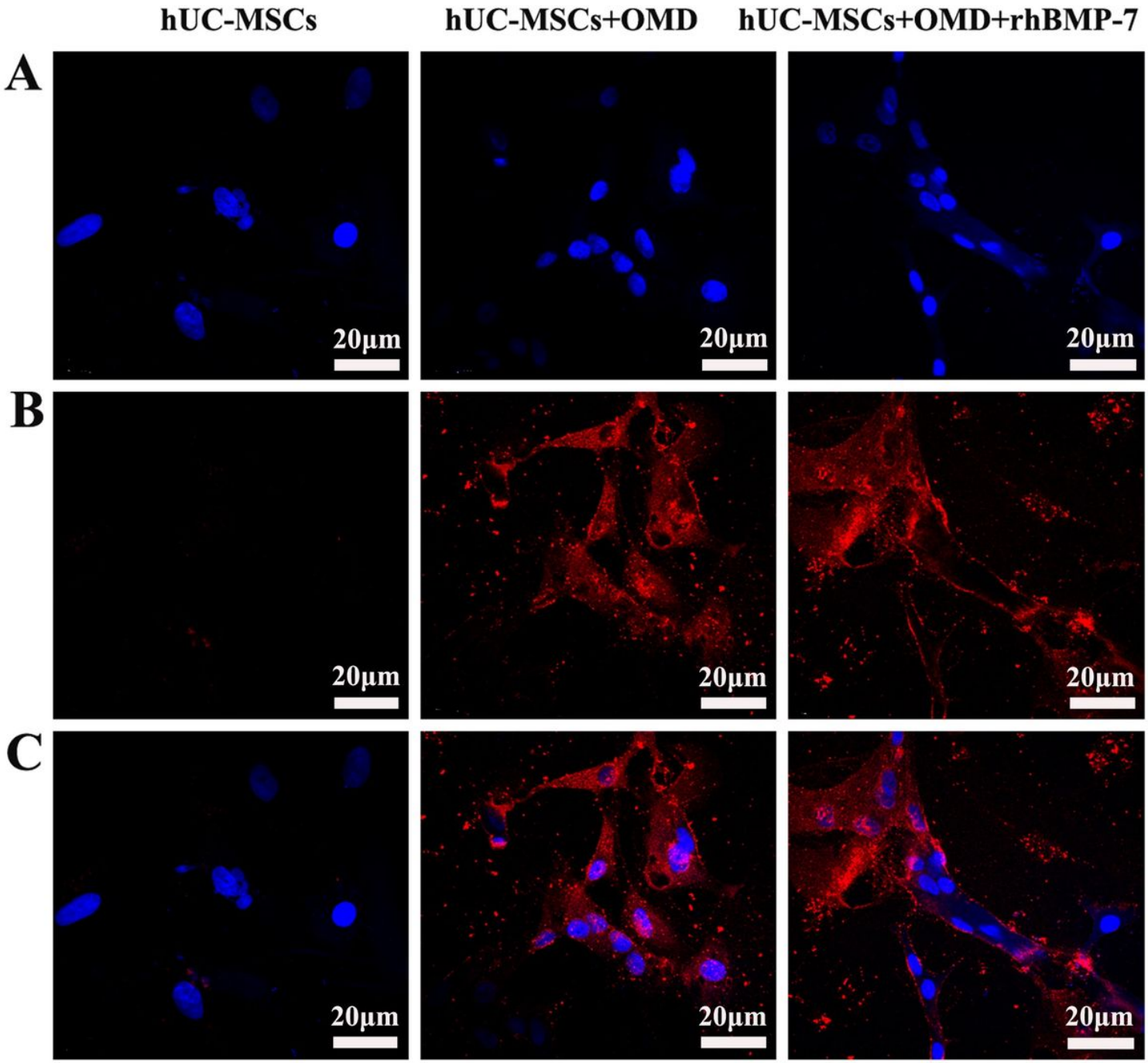

Figure 3

Immunofluorescence staining of OCN in hUC-MSCs on day 14 of culture (scale bar=20 μm). A DAPI. B OCN. C Merge. rhBMP-7 recombinant human bone morphogenetic protein-7, hUC-MSCs human umbilical cord mesenchymal stem cells, OCN osteocalcin, OMD osteogenic media

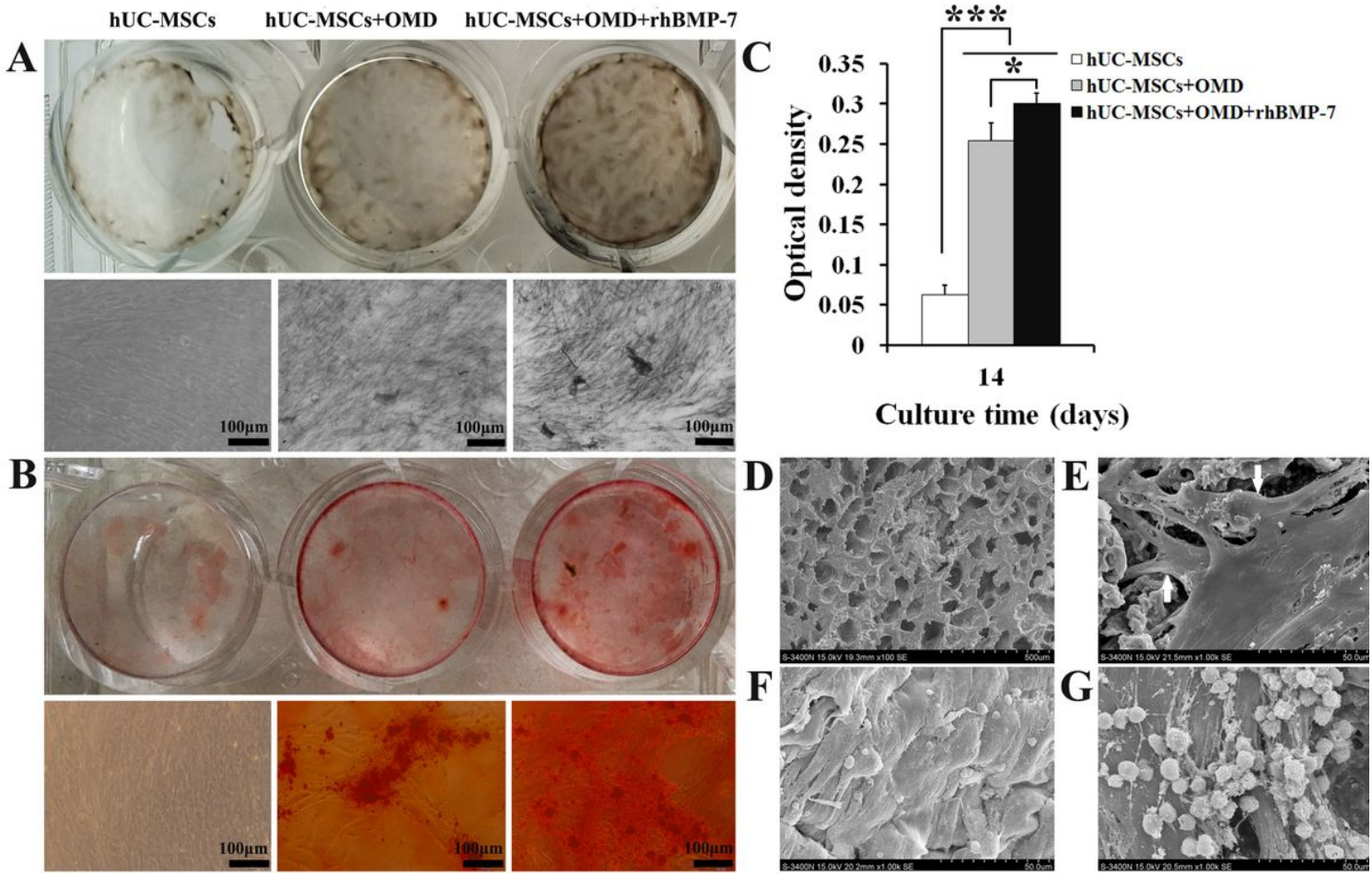

Figure 4

Osteogenic differentiation potential of hUC-MSCs on day 14 of culture and scanning electron microscopy observation of hUC-MSCs combined with nHAC/PLA on day 7 of culture. A Alkaline phosphatase staining (scale bar=100 μm). B Alizarin red staining (scale bar=100 μm). C Mineral formation was measured using a microplate reader (mean ± SD, n=6). *P<0.05, ***P<0.001. D nHAC/PLA (scale bar=500 μm). E hUC-MSCs+nHAC/PLA (scale bar=50 μm). F hUC-MSCs+nHAC/PLA+OMD (scale bar=50 μm). G hUC-MSCs+nHAC/PLA+OMD+rhBMP-7 (scale bar=50 μm). White arrows indicate typical fibroblastic morphology. rhBMP-7 recombinant human bone morphogenetic protein-7, hUC-MSCs human umbilical cord mesenchymal stem cells, nHAC/PLA nano-hydroxyapatite/collagen/poly(L-lactide), OMD osteogenic media

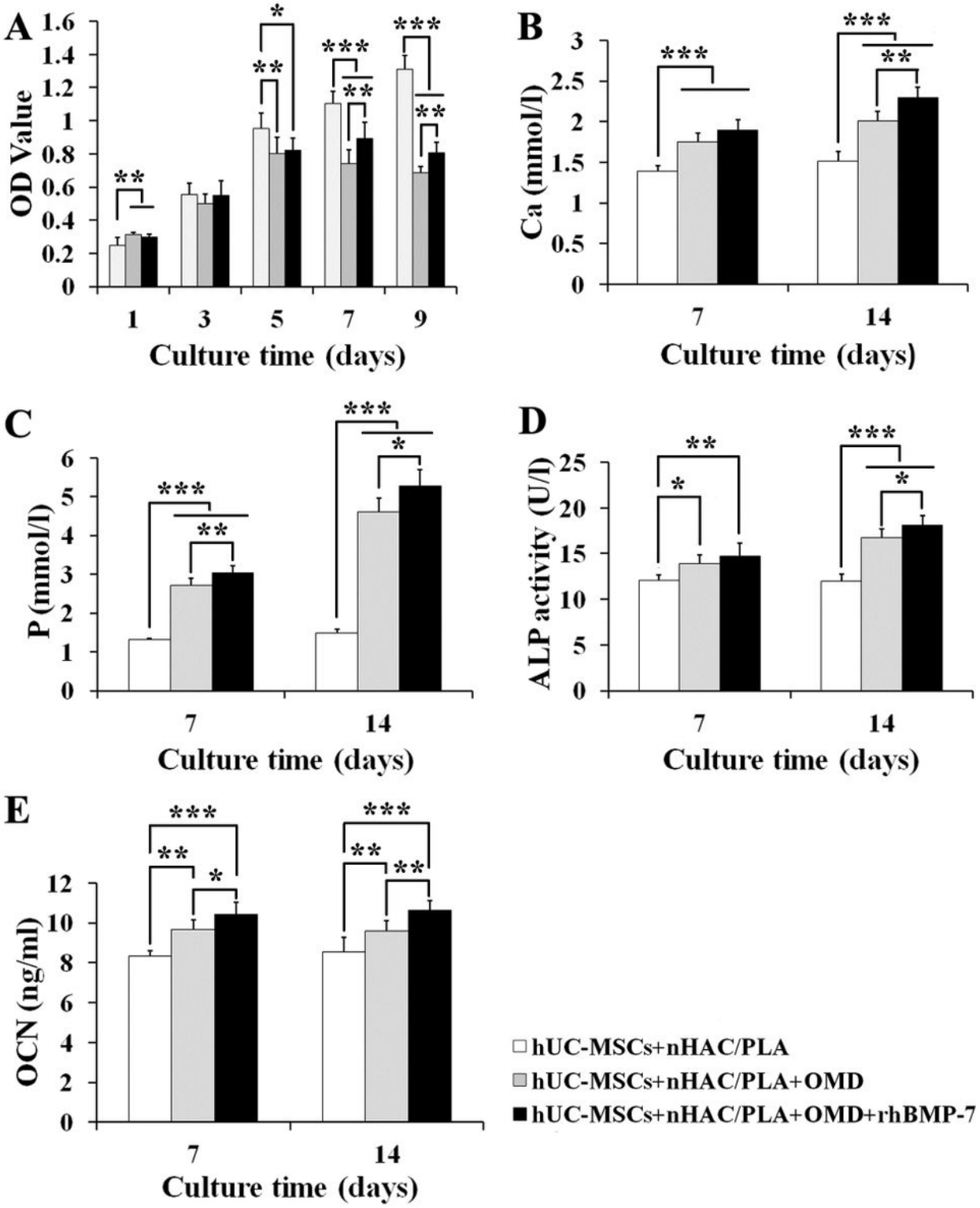

Figure 5

Proliferation and osteogenic differentiation potential of hUC-MSCs combined with nHAC/PLA. The effects of rhBMP-7 on A proliferation (n=8), B Ca concentration, C P concentration, D ALP activity and E OCN concentration. Data are presented as mean ± SD (n=6 or 8). *P<0.05, **P<0.01, ***P<0.001. rhBMP-7 recombinant human bone morphogenetic protein-7, ALP alkaline phosphatase, OCN osteocalcin, hUC-

MSCs human umbilical cord mesenchymal stem cells, nHAC/PLA nano-hydroxyapatite/collagen/poly(L-lactide), OMD osteogenic media, Ca calcium, P phosphorous, OD optical density

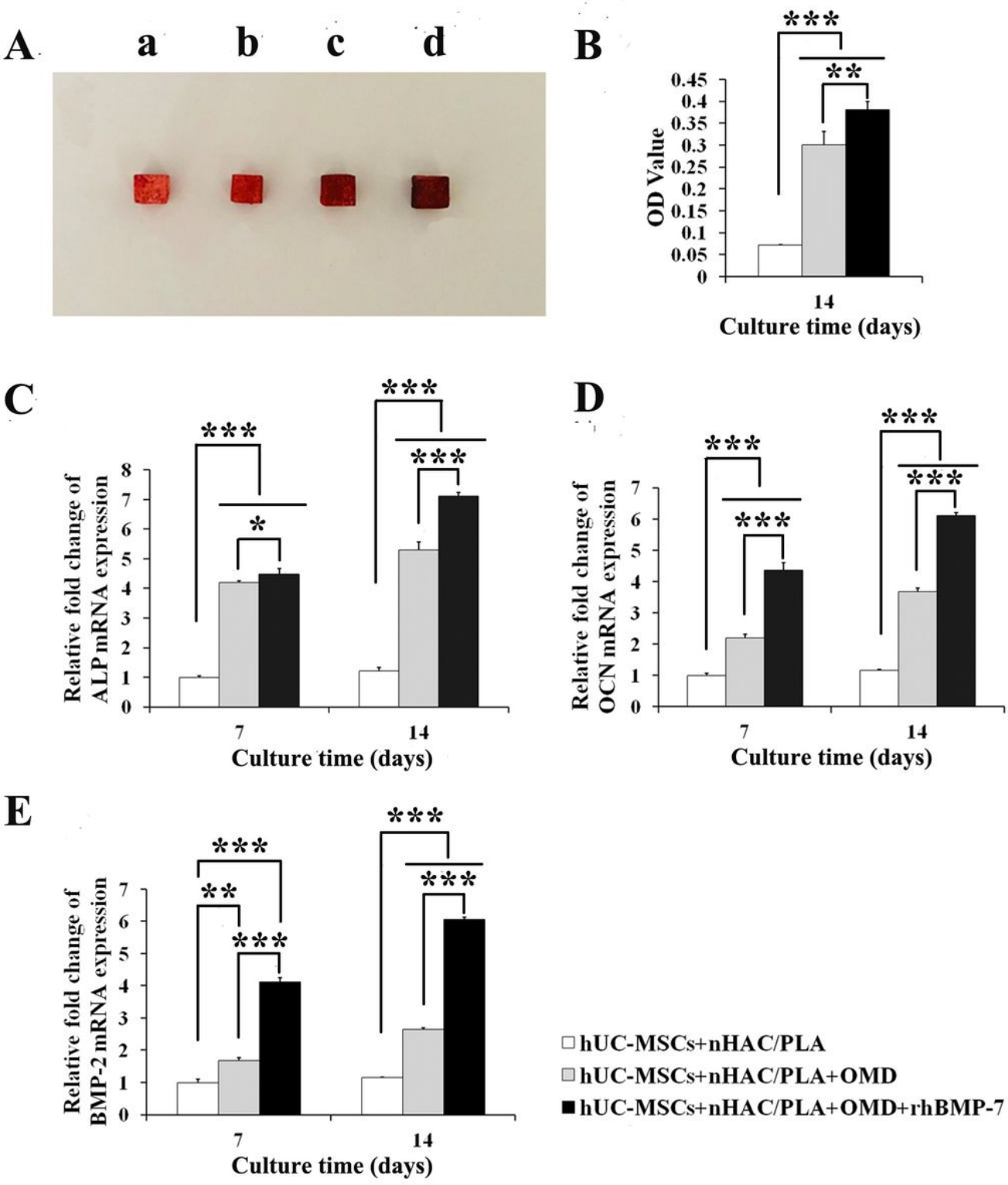

Figure 6

Mineral formation and the mRNA expression of osteogenic differentiation markers in hUC-MSCs combined with nHAC/PLA. A Mineral formation was detected by Alizarin Red staining. (A-a), nHAC/PLA. (A-b), hUC-MSCs+nHAC/PLA. (A-c), hUC-MSCs+nHAC/PLA+OMD. (A-d), hUC-

MSCs+nHAC/PLA+OMD+rhBMP-7. B Mineral formation was measured using a microplate reader (mean ± SD, n=6). The mRNA expression of C ALP, D OCN and E BMP-2 (mean ± SD, n=3). *P<0.05, **P<0.01, ***P<0.001. rhBMP-7 recombinant human bone morphogenetic protein-7, hUC-MSCs human umbilical cord mesenchymal stem cells, nHAC/PLA nano-hydroxyapatite/collagen/poly(L-lactide), OMD osteogenic media, ALP alkaline phosphatase, OCN osteocalcin

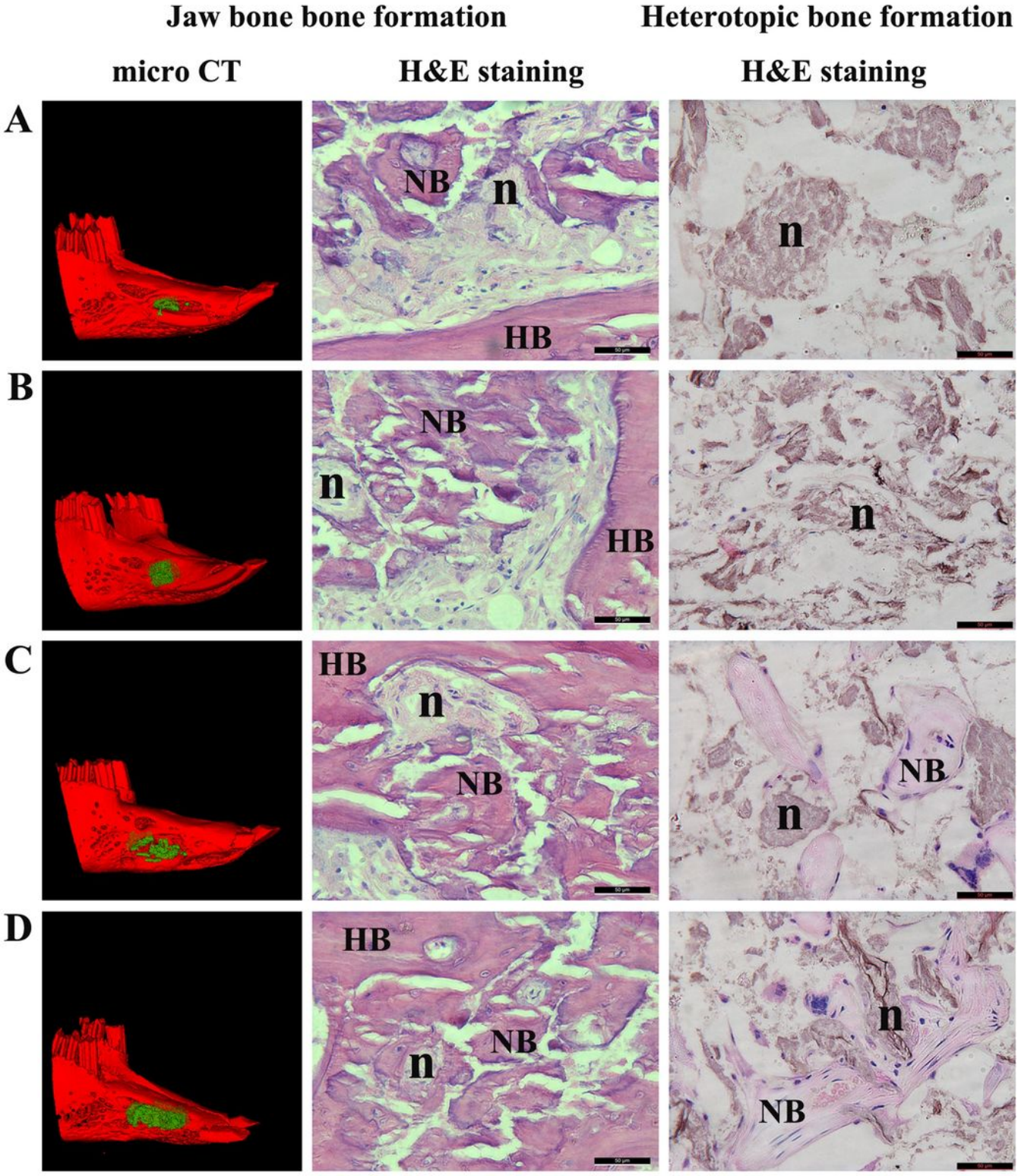

Figure 7

Assessment of bone formation in rabbit jaw bone defect and the back of nude mice after 3 months of surgery. A nHAC/PLA. B hUC-MSCs+nHAC/PLA. C hUC-MSCs+nHAC/PLA+OMD. D hUC-MSCs+nHAC/PLA+OMD+rhBMP-7. Scale bar=50 μm. Green indicated newly-formed bone in micro CT image. HB host bone, NB new bone, n nHAC/PLA. nHAC/PLA nano-hydroxyapatite/collagen/poly(L-lactide), hUC-MSCs human umbilical cord mesenchymal stem cells, OMD osteogenic media, rhBMP-7 recombinant human bone morphogenetic protein-7, H&E staining hematoxylin and eosin staining

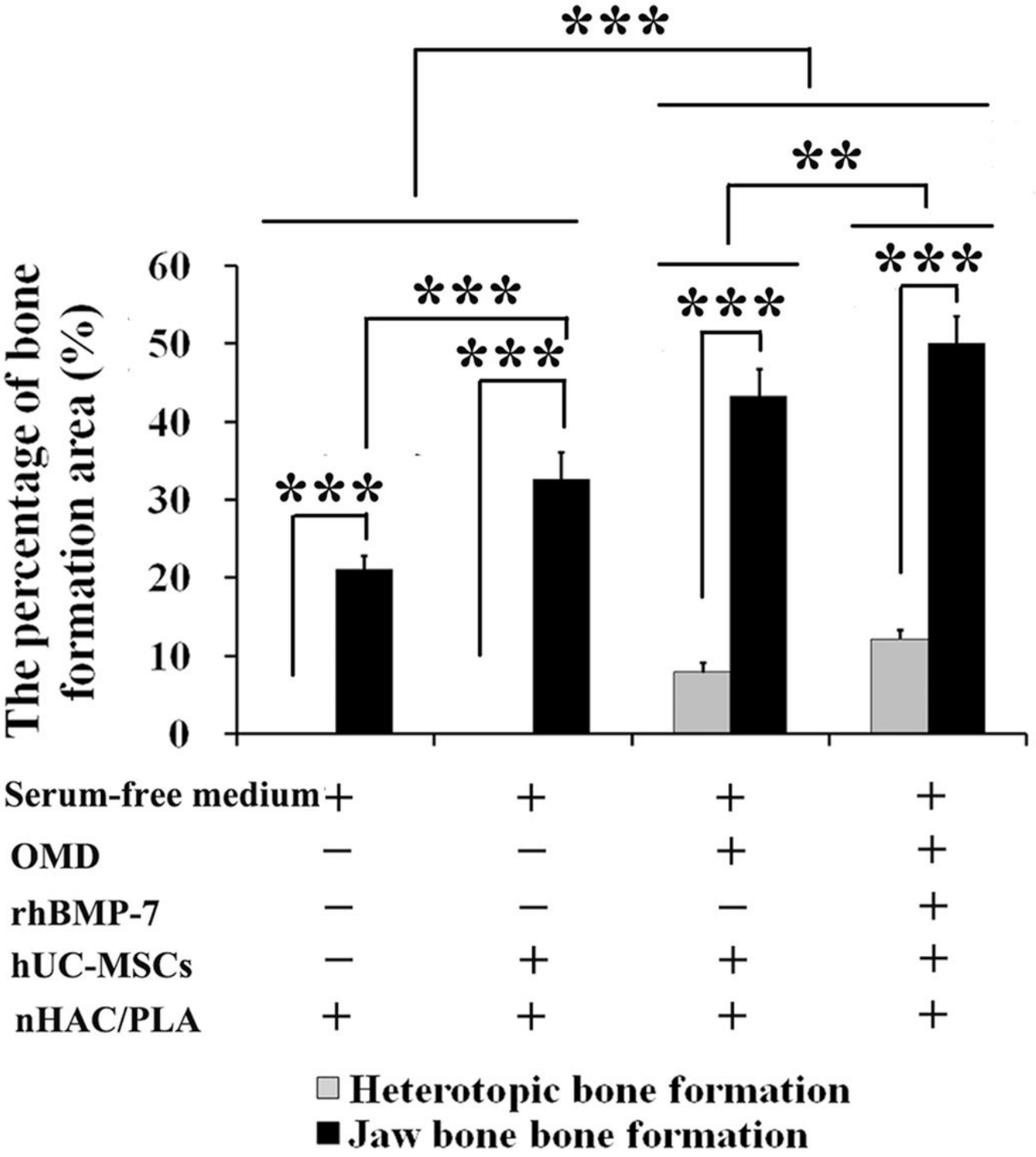

Figure 8

Percentage of bone formation area. Data are presented as mean ± SD (n=6). **P<0.01, ***P<0.001. rhBMP-7 recombinant human bone morphogenetic protein-7, hUC-MSCs human umbilical cord mesenchymal stem cells, nHAC/PLA nano-hydroxyapatite/collagen/poly(L-lactide), OMD osteogenic media

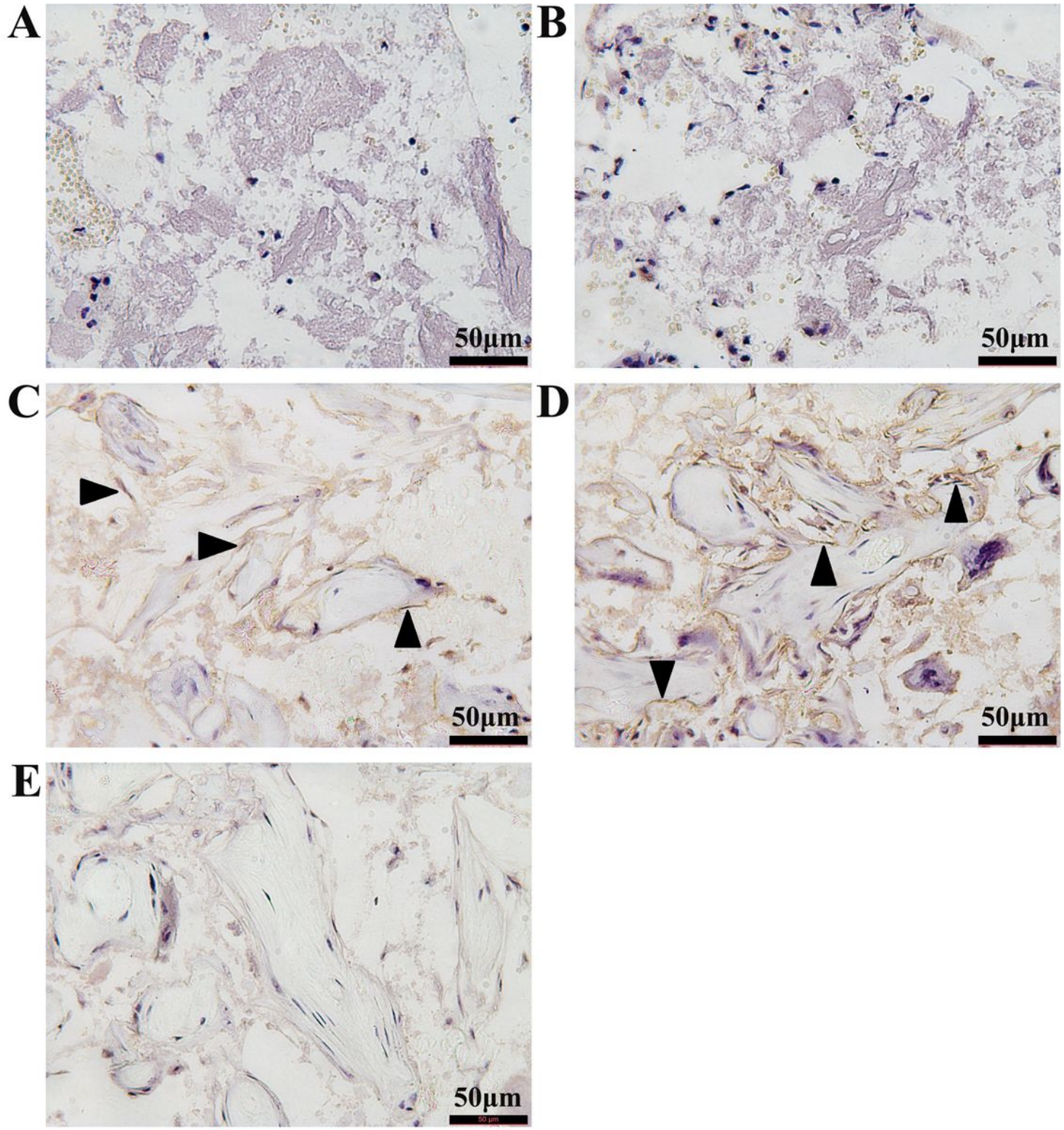

Figure 9

Immunohistochemical staining of OCN in hUC-MSCs combined with nHAC/PLA implanted subcutaneously in the back of nude mice for 3 months. A nHAC/PLA. B hUC-MSCs+nHAC/PLA. C hUC-MSCs+nHAC/PLA+OMD. D hUC-MSCs+nHAC/PLA+OMD+rhBMP-7. E Negative control without incubation with the primary antibody against OCN. Black head arrow indicates an osteoblast positive for OCN. Scale bar=50 μm. rhBMP-7 recombinant human bone morphogenetic protein-7, hUC-MSCs human umbilical cord mesenchymal stem cells, nHAC/PLA nano-hydroxyapatite/collagen/poly(L-lactide), OCN osteocalcin, OMD osteogenic media